



1 **The effect of propagation saw test geometries on critical cut length**

2 Bastian Bergfeld^{1*}, Karl W. Birkeland², Valentin Adam^{1,3}, Philipp L. Rosendahl³, and Alec van Her-
3 wijnen¹

4 ¹ WSL Institute for Snow and Avalanche Research SLF, Davos, Switzerland

5 ² Birkeland Snow and Avalanche Scientific, Bozeman, Montana

6 ³ Institute of Structural Mechanics and Design, Technical University of Darmstadt, Darmstadt, Germany

7 *Correspondence to:* Bastian Bergfeld (bastian.bergfeld@slf.ch)

8

9 **Abstract:**

10 For a slab avalanche to release, a crack in a weak snow layer beneath a cohesive snow slab has to initiate and propagate.
11 Information on crack propagation is essential for assessing avalanche triggering potential. In the field, this information
12 can be gathered with the Propagation Saw Test (PST), a field test that provides valuable data on crack propagation pro-
13 pensity. The first PSTs were performed about 20 years ago and standards have since been established. However, there are
14 still differences in how the PST is performed. Standards in North America require the column ends to be cut vertically,
15 whereas in Europe they are typically cut at a normal angle. In this study, we investigate the effect of these different column
16 geometries on the critical cut length. To this end, we conducted 27 pairs of PST experiments, each pair consisting of one
17 PST with slope normal cut ends and one PST with vertical cut ends. Our experiments showed that PSTs with normal cut
18 ends have up to 50% shorter critical cut lengths, and the difference predominantly depends on the slope angle and slab
19 thickness. We developed two load-based models to convert critical cut lengths between the test geometries: (i) a uniform
20 slab model that treats the slab as one uniform layer and (ii) a layered model that accounts for stratification. For validation,
21 we compare these models with a modern fracture mechanical model. For the rather uniform slabs of our experiments,
22 both load-based models were in excellent agreement with measured data. For slabs with an artificial layering, the uniform
23 load-model predictions reveal deviations from the fracture mechanical model whereas the layered model was still in
24 excellent agreement. This study reveals the influence that the geometry of field tests and the slope angle of the field site
25 have on test results. It also shows that only accurately prepared field tests can be reliable and therefore meaningful.
26 However, we provide models to correct for imprecise field test geometry effects on the critical cut length.

27 **KEYWORDS:** stability test, Propagation Saw Test, edge effect, failure initiation

28 **1 Introduction**

29 Accurate assessment of fracture initiation and crack propagation is essential to evaluate the potential for triggering ava-
30 lanches (Schweizer et al., 2016). In this context, the Propagation Saw Test (PST) is a field test that provides valuable
31 insight into the propensity of cracks to propagate (Gauthier and Jamieson, 2006b). In the past 20 years several studies
32 investigated the influence of PST geometry. They aimed to provide recommendations for the PST column length (Bair
33 et al., 2014) or looked into the effect of changing slab thicknesses (Simenhois and Birkeland, 2008). It was also reported
34 that the critical cut length depends on whether the ends of the PSTs are cut slope-normally or vertically (Gaume et al.,
35 2017). Although PSTs have been used for approximately 20 years and utilized in various studies (Bair et al., 2013;
36 Bergfeld et al., 2022; Bergfeld et al., 2021; Birkeland et al., 2019; Gauthier and Jamieson, 2008b), the lack of widely



37 accepted standards hinders its consistent and reproducible application across locations and practitioners. Standards in
38 North America require the PST column ends to be cut vertically (CAA, 2016; Greene et al., 2022), whereas in Europe
39 they are typically cut at a normal to the slope (Sigrist and Schweizer, 2007; van Herwijnen et al., 2016).

40 This methodological difference could possibly explain why previous studies were not conclusive as to whether the crit-
41 ical cut length decreases (Gaume et al., 2017, slope normal cuts) or increases (Gauthier and Jamieson, 2008a; McClung,
42 2009, both slope vertical cuts) with increasing slope angle. In both, North America and Europe the weak layer is most
43 commonly cut upslope, but in rare cases, the weak layer is also cut downslope from the top. Gauthier and Jamieson
44 (2006a) investigated this difference experimentally and observed no significant dependence of critical cut length on cut-
45 ting direction. However, they also found that critical cut length does not depend on slope angle. Another contradictory
46 statement about the cut length to slope angle relationship. However, the geometric and/or methodological differences of
47 PSTs are likely to affect the results of PSTs (Gaume et al., 2017; Heierli et al., 2008, Supplement Figure S3). Our study
48 aims to investigate the effect of different column geometries and cutting directions on the critical cut length, a major
49 structural property. To achieve this, we conducted a series of side-by-side PST experiments with normal and vertical
50 ends. In addition, we also investigated the influence of cutting direction (upslope or downslope).

51

52 The purpose of these experiments was to demonstrate the influence of PST column geometry and cutting direction on the
53 critical cut length. We also explain where these differences come from and how the stratification of the snowpack influ-
54 ence these geometric effects. To this end, we developed a uniform- and layered load-based models to convert between
55 PST geometries. In addition, the developed conversion models were validated against a modern fracture mechanics model
56 (Rosendahl and Weissgraeber, 2020; Weißgraeber and Rosendahl, 2023).

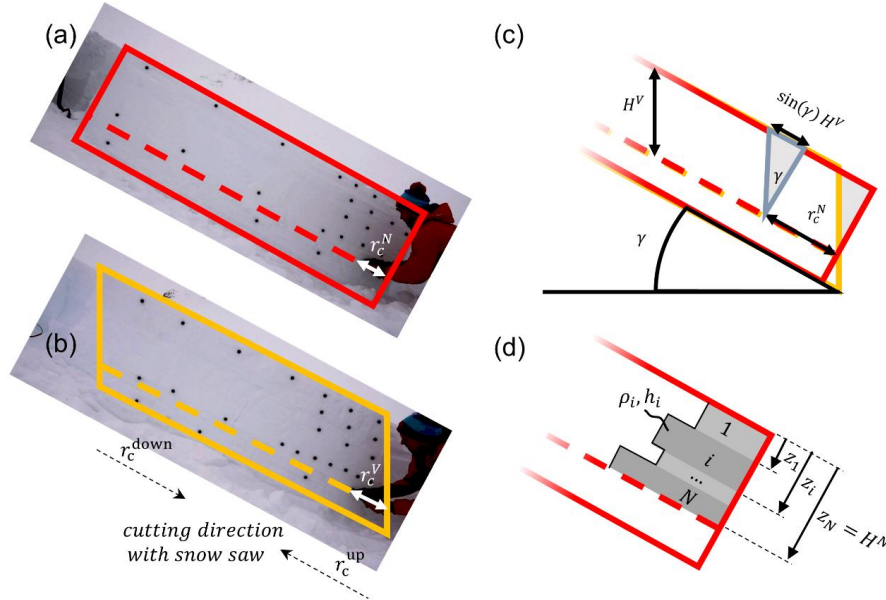
57 **2 Methods**

58 **Field Experiments**

59 In January and March 2021, we performed field experiments above Davos in the Eastern Swiss Alps, and in Montana,
60 United States. All field sites were around 2400 m.a.s.l. and PSTs resulted in all possible propagation outcomes (slab
61 fracture, crack arrest and full propagation). In Davos, we tested a weak layer consisting of surface hoar (grain size: 2-4
62 mm), while in Montana the weak layer consisted of depth hoar (grain size: 1-4 mm) (Fierz et al., 2008). Slab thickness
63 ranged from 52 to 96 cm.

64

65 In total 27 pairs of PSTs were performed, with each pair consisting of one test using slope normal ends (results with
66 superscript X^N , Figure 1a) and the other with vertical ends (superscript X^V , Figure 1b). For 6 pairs we also performed
67 pairs of PSTs in which the weak layer was cut in upslope as well as in downslope direction (r_c^{up} and r_c^{down} in Figure 1b).



68

69

70 **Figure 1:** (a) PST with normal ends and a critical cut length r_c^N . The red outline indicates the PST geometry. The dashed line
 71 indicates the height of the weak layer. (b) PST with vertical ends and a critical cut length r_c^V . (c) Difference in PST geometry.
 72 The main difference is the additional slab load for the slope normal geometry shown by the grey triangle. H^V is the vertical
 73 measured slab thickness and γ the slope angle. (d) In the layered load conversion model, each slab layer i contributes according
 74 to their density ρ_i , layer thickness h_i and depth in the slab z_i .

75 For all PSTs, we recorded the critical cut length as r_c^N for PSTs with normal ends, and r_c^V for vertical ends. We then
 76 compute the ratio of both cut lengths r_c^V/r_c^N . To investigate the effect of cutting directions, we used the ratio $r_c^{\text{up}}/r_c^{\text{down}}$,
 77 where r_c^{up} and r_c^{down} indicate whether the critical cut length was taken from upslope or downslope cutting of the weak
 78 layer, respectively (Figure 1b).

79 Conversion Models

80 **Uniform Load Model (ULM).** To find a relationship between r_c^N and r_c^V , we assume that the ratio of the cut lengths is
 81 inversely proportional to the ratio of the loads of the unsupported slab above the saw cut:

$$82 \quad \frac{r_c^V}{r_c^N} \propto \frac{\sigma^N}{\sigma^V} = 1 + \frac{\sin(\gamma) H^V}{2r_c^N} \quad (1)$$

83 If the loads σ^N and σ^V are expressed through snowpack properties and a uniform slab is assumed, the expression on the
 84 right-hand side is obtained, where H^V is the vertically measured slab thickness and γ the slope angle. Other snow and
 85 geometrical properties (e.g., slab density, beam width, etc.) cancel out. With $H^V = \cos(\gamma) H^N$, where H^N is the slope
 86 normal slab thickness, equation 1 results in the following model for the conversion of critical cut lengths (assumption of
 87 a uniform slab):

$$88 \quad r_c^V = r_c^N + \frac{\tan(\gamma) H^N}{2} \quad (2)$$



89 At this point we would like to point out that this relationship (Equation 2) was already suggested in the context of anticrack
90 nucleation. However, the derivation was based purely on geometric considerations and no further verification was carried
91 out (Heierli et al., 2008, Supplement Figure S3).

92 **Layered Load Model (LLM).** The temporal sequence of weather conditions inevitably produces layered slabs in a nat-
93 ural snowpack. The individual layers differ, among other parameters, in their layer thickness and density. A sloped PST
94 with layered slab in slope normal geometry results in more (compared to the ULM) load above the saw cut if high density
95 layers are close to the snow surface (grey triangle in (Figure 1c and d). In addition to the slope angle γ , the extra load
96 depends on the individual layer thickness h_i , density ρ_i , and on the relative depth z_i within the slab (Figure 1d). Concep-
97 tually, the layered load model is based on the same assumptions as the uniform load model. However, it considers the
98 layering which makes the formulation to compute the additional load of PSTs with slope normal geometry more intricate:

$$99 \quad r_c^V = \frac{\sum_{i=1}^N r_c^N h_i \rho_i + \frac{\tan(\gamma)}{2} h_i^2 \rho_i + \tan(\gamma) (z_N - z_i) h_i \rho_i}{\sum_{i=1}^N h_i \rho_i} \quad (3)$$

100 Where N is the number of layers. For a detailed derivation of the layered load model we refer to Appendix A.

101

102 **Layered Mechanical Model (LMM).**

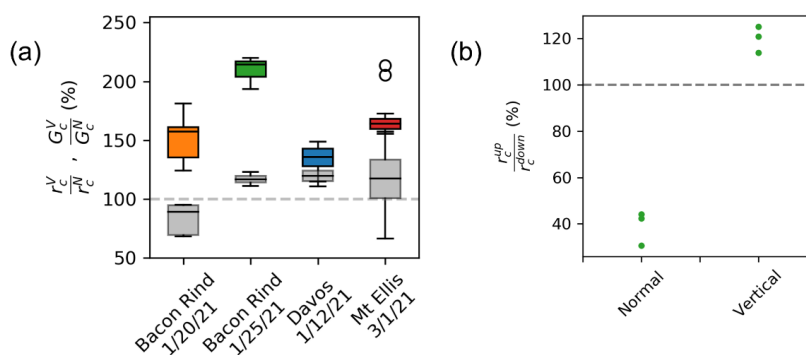
103 For further verification of the load models, we use a closed-form analytical model for layered snowpacks (Weißgraeber
104 and Rosendahl, 2023) that was recently validated with field data (Bergfeld et al., 2023), has been utilized. This model
105 describes the slab as shear-deformable, layered beam, and allows cylindrical bending, while the weak layer is represented
106 as a layer of smeared springs. We used the model to determine the critical energy release rate G from the measured critical
107 cut length, depending of the geometric configuration (G_c^N or G_c^V , respectively). This critical energy release rate, also called
108 specific fracture energy, is a material property of the weak layer describing its resistance to crack growth, and it is hence
109 a proxy for the fundamental physical process of crack growth in PSTs. Subsequently, we used the critical energy release
110 rate determined from an experiment with slope normal beam ends to calculate back to the critical cut length of a vertically
111 cut PST. This model is therefore also suitable to convert a critical cut length measured in one PST configuration to another.
112 Compared to the ULM (Equation 2) and the LLM (Equation 3), the LMM requires many more snowpack properties.
113 However, it represents the specific snowpack layering of a PST and its influence on the critical cut length in much more
114 detail, as it takes into account the full deformation behaviour of the slab and weak layer system. We therefore used the
115 LMM to verify the influence of an asymmetrically layered slab on our load-based models (ULM, LLM).

116 Results

117 In total we performed 66 PSTs at four different field sites. 54 PSTs aimed to investigate the effect of PST geometry
118 (Appendix, Table C1), therefore the dataset include 27 pairs of PSTs and each pair consists of one PST with slope normal
119 and one with vertical PST beam ends. The remaining 12 PSTs were performed to investigate the difference between
120 upslope- and downslope cutting of a PST (Appendix, Table C2).

121 Normal vs. vertical PST ends

122 Critical cut lengths were measured between 14 and 70 cm. Overall, r_c^V was systematically larger than r_c^N , on average
123 almost 50 % (colored boxes in Figure 2a).



124

125 **Figure 2: (a) Ratio of critical cut lengths shown as boxplots for the different field days (colored). Ratio of the critical energy**
 126 **release rates computed with the mechanical model using the critical cut lengths of the experiments (grey). Boxes represent the**
 127 **inter-quartile range with the middle line representing the median value. (b) Ratio of critical cut length from PSTs with**
 128 **downslope and upslope cuts. Results are shown for PSTs with normal and vertical PST ends. Both: The dashed line represents**
 129 **a ratio of 1.**

130 Differences in snowpack conditions at the various field sites resulted in different deviations between PST geometries.

131 Median ratios ranged from 136 % to 214 % (Figure 2a, horizontal lines in the colored boxes).

132 **Upslope vs. Downslope cutting**

133 Beside PST geometry, the cutting direction also affects the critical cut length. For PSTs with normal ends, r_c^{up} was about

134 40% of r_c^{down} (Figure 2b, left), while for vertical PST ends r_c^{up} was about 20% longer than r_c^{down} (Figure 2b, right).

135 Again, these rather large differences can be explained by slab loading and slab mechanics as will be detailed in the dis-

136 cussions section.

137 **Models**

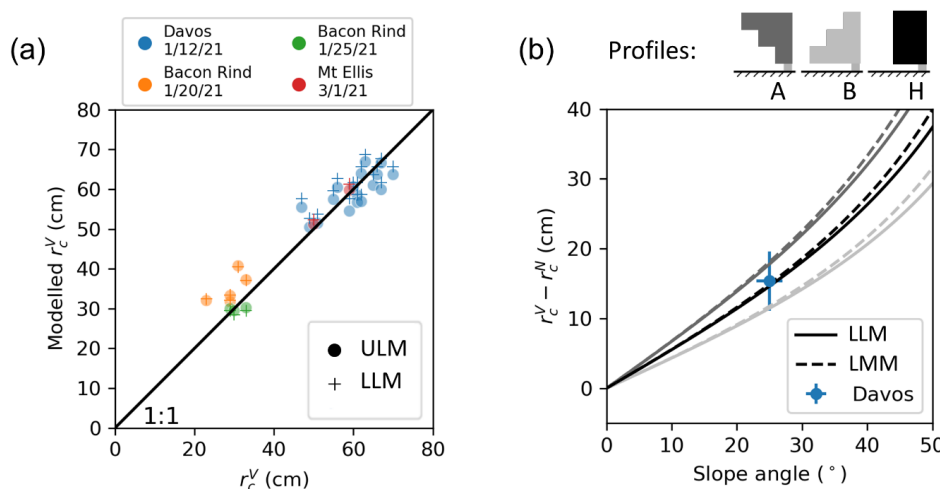
138 With Equations (2) and (3) we provide a **uniform load model** and a **layered load model**, respectively. The models allow

139 us to convert critical cut lengths between the different PST geometries. Our experiments show very good agreement with

140 both the uniform-load model (Figure 3a, dots) and the layered load model (Figure 3a, crosses). The RMSE between the

141 measured critical cut lengths in vertical geometry r_c^V and the modelled counterpart is 4.4 cm for the uniform load model

142 and 4.6 cm for the layered load model.



143

144 **Figure 3:** (a) Modelled critical cut lengths for upslope cuts with vertical PST geometry r_c^V with the corresponding measured
 145 values, dots represent the uniform load model (ULM, Equation 2) and pluses the layered load model (LLD, Equation 3). Dif-
 146 ferent colors indicate the different field days. The black line is the 1:1 line and indicates a perfect model. (b) Modelled differ-
 147 ences in critical cut lengths with slope angle. The blue dot represents the mean and uncertainty of the measurements in Davos,
 148 as this field day served to define the artificial profiles by matching the mean density. The solid lines are the layered load model
 149 and the dashed lines result from the layered mechanical model (LMM). The grey shades indicate different slab profiles given
 150 at the top of the figure.

151 Using the **layered mechanical model** to analyse the global energy balance at the onset of crack growth, we derived
 152 critical energy release rates from the experimental data. The model considers the layering and geometrical configuration
 153 of a PST experiment to determine the critical energy release rate at the critical cut length, i.e., the specific fracture energy.
 154 Unlike the critical cut length, the critical energy release rate is a material property of the weak layer and should thus not
 155 depend on test geometry. In fact, the determined critical energy release rates, measured in the different PST configurations
 156 (vertical or normal beam ends), differed by a maximum of 20% (Figure 2a, grey boxes), whereas the deviations of the
 157 critical cut length were up to six times larger (Figure 2a, coloured boxes).

158

159 Our **uniform load model** considers a homogeneous slab and gives a tangential slope dependence (see Equation 2 and
 160 black solid line in Figure 3b). For comparison, the **layered load model** and the **layered mechanical model** were evaluated
 161 for many different slope angles (Figure 3b, solid and dashed lines, respectively) and 3 different generic slab configurations
 162 (Figure 3b, top). In profile H the mean slab density matched the observed snow cover at our experiments in Davos. The
 163 direct comparison for the artificial profile H shows a very good agreement between the load models and the mechanical
 164 model (compare black solid line and black dashed line in Figure 3b). Note that for profile H the two load models are
 165 equal. The deviations of the critical cut lengths ($r_c^V - r_c^N$) measured in Davos can be reproduced very accurately with all
 166 models (Figure 3b, black lines and blue dot). In the asymmetric profiles A and B, additional artificial layers with the
 167 minimum and maximum density of the Davos snow profile were inserted. For these highly asymmetric slabs (grey lines
 168 in Figure 3) there are deviations between the models. Of course, the uniform model cannot represent any differences
 169 induced by the layering. However, the layered load model and the mechanical model show good agreement over the entire
 170 angle range, whereby the deviations slightly increase with increasing slope angles.



171 **Discussion**

172 **Normal vs. vertical PST ends**

173 PSTs with slope-normal and vertical ends showed large differences in the measured critical cut length. These differences
174 can be explained with the different PST geometries and the corresponding slab-induced loading of the weak layer. We
175 assume that PST beams were long enough, so that the tail end of the PST beam remains mechanically unchanged when
176 the saw cut is increased and is therefore not relevant (Bair et al., 2014). The constellation is as shown schematically in
177 Figure 1c. Even with no saw cut, the slope normal PST geometry already has an "unsupported" portion of the slab above
178 the weak layer (Figure 4a, blue area at the right beam end). This additional load, in normal geometry, generates higher
179 stresses in the weak layer (and higher energy release rate), leading to shorter critical cut lengths. The shorter critical cut
180 lengths can therefore easily be attributed to this additional load. However, the extent of the difference depends on snow-
181 pack properties (e.g. slab thickness, density layering) and slope angle.

182

183 This emphasizes that a measured critical cut length can only be interpreted for stability assessment if the applied geometric
184 PST configuration (including slope angle) is considered. In other words, our data show that two equal snowpacks, which
185 should exhibit a similar crack propagation propensity, likely result in completely different critical cut lengths depending
186 on how the PST beam ends were cut and on which slope angle the PST was performed. To ensure comparability of
187 measured critical cut lengths, it is thus imperative to account for the geometrical configuration and snowpack layering,
188 using the models presented.

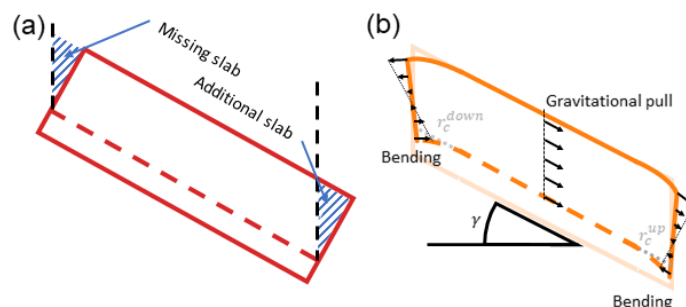
189 **Upslope vs. Downslope cutting**

190 When cutting upslope, there is an additional part of the slab that induces an extra load on the weak layer in the normal
191 configuration (Figure 4a, blue area at the right beam end). When cutting from the top, however, a part of the slab is
192 missing, and there is less load (Figure 4a, blue area at the left beam end). The critical cut length of the upslope cut is thus
193 much shorter, in our experiments about 60% shorter (left side in Figure 2b).

194

195 In the vertical configuration, on the other hand, the load over the saw cut is always the same, independent of the cutting
196 direction. The observed differences, however, come from the differences in shear stress at the crack tip. Indeed, at the
197 weak layer, there are two shear stress components: (i) shear stress from the slope parallel gravitational pull on the slab
198 (Figure 4b, arrows in the middle), and (ii) bending induced shear stresses (Figure 4b, arrows at the left and right beam
199 end). The slope parallel gravitational pull is always in the same direction (downslope). The bending induced shear stresses
200 at the height of the weak layer, on the other hand, are always in the cut direction. When cutting the weak layer from the
201 bottom upwards, both contributions thus have an opposite effect and partially cancel each other out, while when cutting
202 from the top, both shear stresses have the same sign and add up. This results in longer critical cut lengths when sawing
203 upslope in vertical PSTs. In our measurements, these were 20% longer (right side in Figure 2b).

204



205

206 **Figure 4:** (a) Schematic representation of a PST with normal ends and without a saw cut. The blue marked areas, at the right
 207 and left of the PST beam, indicate the additional and missing slab load, respectively, relative to vertical ends (black dashed
 208 lines). (b) PST with vertical ends and critical cut lengths r_c^{up} and r_c^{down} for upslope and downslope cutting, respectively. At
 209 both PST beam ends the saw cut leads to bending, which results in a stress profile across the slab thickness (black arrows). In
 210 the middle part of the PST, the black arrows represent stress in the slab due to the slope parallel gravitational pull. γ is the
 211 slope angle.

212

213 Models

214 Overall, the load models effectively explained our field results. (Figure 3a). If the RMSE of the uniform load- and layered
 215 load model is compared, the uniform load model performs slightly better than the layered load model. However, since
 216 our snowpack profiles show relatively homogeneous slabs without pronounced asymmetry (see Appendix D), we would
 217 not attach any significance to this minor difference, especially for inhomogeneous and asymmetrical slabs. We believe
 218 the layered load model is more accurate. This becomes clear in Figure 3b. Profiles A and B have a density gradient within
 219 the slab (asymmetry). Deviations between the uniform and the layered load model seem plausible as higher density layers
 220 which are close to the snow surface contribute more to the additional load present in slope normal PSTs (blue hashed in
 221 Figure 4a) than if they are deeper in the snowpack. The difference in critical cut lengths is expected to be larger (profile
 222 A) or smaller (profile B) than predicted by the uniform load model.

223

224 Beside the overall good conversion performance of the models, a systematic offset for PSTs from 20 January 2021 seem
 225 to be present (orange dots in Figure 3). We suspect that in these PSTs the beam length was too short, the ratio between
 226 slab thickness and beam length was only about 0.5. It is therefore very likely that the geometric difference at the tail end
 227 of the beam was also relevant (Bair et al., 2014). However, this is not considered in the models. Overall, our results thus
 228 show that the PST geometry plays an important role in the measured critical cut length, and this is mostly driven by
 229 differences in load from the slab.

230

231 Model application and limitation:

232 PST datasets with different PST configurations can be homogenised using our models. This will increase the comparability
 233 and ultimately the scientific utility of these datasets. In addition, it is often the case that the PST ends are cut
 234 imprecisely (not perfectly vertical or slope normal) on inclined terrain. The angle of the free edge can easily be determined
 235 from photos of the test, and a correction can then be applied using one of the load models with minor modifications
 236 (Appendix B). The scatter of the experimentally determined critical cut lengths should thus be reduced.



237 Beside applications, shortcomings of the suggested load models are evident. The suggested load models rely on Equa-
238 tion 1, rearranged it reads to: $r_c^V \sigma^V \propto r_c^N \sigma^N$. Using equation A2 (Appendix A) the unit on both sides of the relation is
239 J/m^2 , an energy per unit area. The interpretation of Equation 1 is similar to equating both PST configurations (vertical
240 and normal cut ends) by the specific fracture energy of the weak layer, which is a reasonable approach followed by the
241 layered mechanical model. However, equation 1 remains freely chosen because it is not the fracture energy that is com-
242 puted by $r_c^X \sigma^X$. Our experimental results show that the relationship is sufficiently accurate for the conversion of PST
243 geometries. However, if there are additional changes beyond the PST geometry, the relationship may no longer be suffi-
244 cient. Imagine additional terms from factors A and contributions B in Equation 1:

$$245 A(\gamma, H^N, \dots) r_c^V \sigma^V + B(\gamma, H^N, \dots) \propto A(\tilde{\gamma}, \tilde{H}^N, \dots) r_c^N \sigma^N + B(\tilde{\gamma}, \tilde{H}^N, \dots)$$

246 Both can have functional relationships on properties such as slope angle ($\gamma, \tilde{\gamma}$) and slab thickness (H^N, \tilde{H}^N).

247 As long as such properties remain unchanged ($\gamma = \tilde{\gamma}, H^N = \tilde{H}^N$), the additional terms cancel each other out and our load
248 models are applicable.

249 However, if the critical cut length measured at a certain slope angle and snow cover has to be transferred to a different
250 situation, the applicability of our models still needs to be confirmed with more experimental work. If necessary, the
251 functional relationships A and B will probably have to be identified and added. A more generally valid conversion for
252 critical cut lengths would be of great practical benefit as it allows to extrapolate measured point information on crack
253 propagation propensity to other slope areas were experimental work is not possible.

254 Conclusion and Outlook

255 This work has shown that the result of a PST, i.e., the measured critical cut length, is strongly influenced by the test
256 geometry and cutting direction. PSTs with slope normal beam ends systematically produce shorter critical cut lengths
257 (48% on average). It also makes a significant difference whether the saw cut in a PST is made in the upslope or downslope
258 direction (deviations up to 60%). Both deviations can be explained mechanically and are largely controlled by the differ-
259 ence in slab induced loads. Based on the slab load, a load model was derived for uniform, as well as for layered slabs.
260 Both models agree well with the experimental results. The comparison with a more sophisticated validated fracture me-
261 chanical model shows good agreement between all models as long as the slab is largely homogeneous. For layered slabs,
262 the uniform load model shows greater deviations. The layered load model, on the other hand, shows only minor deviations.
263 This demonstrates that the fracture mechanical model (LMM) is also largely load-driven in this specific application.
264 Overall, our results show that the interpretation of measured critical cut length in a PST is not straightforward, as it is
265 influenced by weak layer properties (specific fracture energy), slab properties (e.g. layering), and test geometry.

266
267 Based on our findings, we suggest that PSTs with slope normal ends should be performed with a saw cut in the upslope
268 direction (Figure 1a). This will ensure that the recorded cut lengths are as short as possible and that the overall test
269 geometry, particularly the column length, has less influence on the test result. However, this has the disadvantage that the
270 effects of slope angle are greater than for vertically cut PSTs. In order to compare tests on different slopes, this effect
271 must be compensated for, which is not straight forward yet. For research purposes, therefore, experiments need to be post-
272 processed before results from different snow packs, slope inclinations, etc. are compared or combined.



273 However, if the PST is to be used as a stability tool without further investigation, the vertical PST configuration should
 274 be preferred by practitioners as it allows results to be extrapolated from flatter terrain to steeper slopes with less error.

275

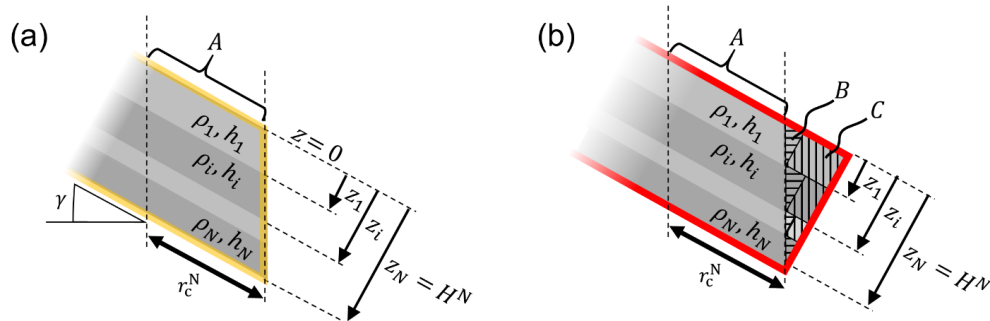
276 In general, the use of consistent PST standards will ensure that PST results are easy to interpret, will ensure scientific
 277 rigor and will improve the comparability of tests and their results. In addition, standardization and conversion models
 278 facilitate the comparison of results between researchers, leading to a deeper understanding of snowpack behavior. Prac-
 279 titioners also benefit from standardized methods and interpretation aids that are invaluable in assessing avalanche risk
 280 based on stability tests.

281

282 **Appendix A:**

283 The load above the saw cut of a PST with slope vertical geometry (V-PST) is independent of the slope angle. However,
 284 the load of a PST with slope normal edges (N-PSTs) is not. In sloped terrain, a N-PSTs has more load above the saw cut
 285 than a V-PST. The difference depends on the slope angle, but the layering also has an influence. Layers close to the snow
 286 surface contribute more to the extra load than layers close to the weak layer (of the saw cut). In order to express the
 287 relationship between critical cut lengths r_c^V , r_c^N and loads σ^V , σ^N (Equation 1, main manuscript) the loads of layered
 288 snowpacks have to be formulated through density ρ_i , thickness h_i and the vertical location z_i of the slab layers i (Figure
 289 A1).

290



291

292 **Figure A1:** (a) Schematic representation of a layered slab in a PST with slope vertical geometry (V-PST). (b) PST with slope
 293 normal geometry (N-PST). In both cases the load above the saw cut r_c^N depends on the density ρ_i and thickness h_i of the slab
 294 layers i . In (b), the load of the N-PST depends additionally on the slope angle as the areas B and C increase with increasing
 295 angle.

296 First for the simpler case of a V-PST (Figure A1a) the mass and load is given by:

297

$$m_A = r_c^V b \sum_{i=1}^N h_i \rho_i \quad (A1)$$

298

$$\sigma^V = \frac{m_A g}{r_c^V b} = g \sum_{i=1}^N h_i \rho_i \quad (A2)$$

299



300 Where g is the gravitational acceleration and b is the width of the PST. In the N-PST the Volumes B and C also contribute
 301 to the overall mass located above the saw cut:

$$302 \quad \sigma^N = \frac{(m_A + m_B + m_C)g}{r_c^N b} \quad (A3)$$

303 The mass of Volume A remains the same as in Equation A1. The masses m_B and m_C are given by:

$$304 \quad m_B = \frac{1}{2} h_1^2 \tan(\gamma) b \rho_1 + \frac{1}{2} h_2^2 \tan(\gamma) b \rho_2 + \dots + \frac{1}{2} h_N^2 \tan(\gamma) b \rho_N = \frac{b \tan(\gamma) \sum_{i=1}^N h_i^2 \rho_i}{2} \quad (A4)$$

$$305 \quad m_C = (z_N - z_1) \tan(\gamma) h_1 b \rho_1 + (z_N - z_2) \tan(\gamma) h_2 b \rho_2 + \dots + (z_N - z_N) \tan(\gamma) h_N b \rho_N$$

$$306 \quad = b \tan(\gamma) \sum_{i=1}^N (z_N - z_i) h_i \rho_i \quad (A5)$$

307 Putting this together results in the overall mass of:

$$308 \quad m_A + m_B + m_C = \tan(\gamma) b r_c^N \sum_{i=1}^N \frac{h_i \rho_i}{\tan(\gamma)} + \frac{h_i^2 \rho_i}{2 r_c^N} + \frac{(z_N - z_i) h_i \rho_i}{r_c^N} \quad (A6)$$

309

310 Inserting in Equation A3 provides:

$$311 \quad \sigma^N = \tan(\gamma) g \sum_{i=1}^N \frac{h_i \rho_i}{\tan(\gamma)} + \frac{h_i^2 \rho_i}{2 r_c^N} + \frac{(z_N - z_i) h_i \rho_i}{r_c^N} \quad (A7)$$

312 As a result, the layered load model provides the relation between the critical cut lengths r_c^V and r_c^N :

313

314

$$315 \quad \frac{r_c^V}{r_c^N} \propto \frac{\sigma^N}{\sigma^V} = \frac{\tan(\gamma) \sum_{i=1}^N \frac{h_i \rho_i}{\tan(\gamma)} + \frac{h_i^2 \rho_i}{2 r_c^N} + \frac{(z_N - z_i) h_i \rho_i}{r_c^N}}{\sum_{i=1}^N h_i \rho_i} \quad (A8)$$

316

$$317 \quad r_c^V = r_c^N \frac{\tan(\gamma) \sum_{i=1}^N \frac{h_i \rho_i}{\tan(\gamma)} + \frac{h_i^2 \rho_i}{2 r_c^N} + \frac{(z_N - z_i) h_i \rho_i}{r_c^N}}{\sum_{i=1}^N h_i \rho_i}$$

$$318 \quad = \frac{\sum_{i=1}^N r_c^N h_i \rho_i + \frac{\tan(\gamma)}{2} h_i^2 \rho_i + \tan(\gamma) (z_N - z_i) h_i \rho_i}{\sum_{i=1}^N h_i \rho_i} \quad (A9)$$

319

320 **Appendix B:**

321 The equations derived in appendix A can be used to formulate a model to correct for imprecisely cut PST beam ends. E.g.
 322 the sawing edge of a PST was close to cut slope normal, but with a deviation of angle β from slope normal (or vertical).

323 As a result, the critical cut length $r_c^{\tilde{N}}$ is measured in such an experiment. To account for this deviation, we have to add a
 324 mass m_D in Equation A6. Note that this “mass” can be negative in the case β is negative (less overhanging mass than the
 325 slope normal cut). The mass m_D has the same contributions as m_B and m_C but is computed from the angle of error β :

$$326 \quad m_D = \frac{b \tan(\beta) \sum_{i=1}^N h_i^2 \rho_i}{2} + b \tan(\beta) \sum_{i=1}^N (z_N - z_i) h_i \rho_i \quad (B1)$$

327 At the end, the ratio of the loads and the relation of the cut lengths is given by:



328

329

$$330 \quad \frac{r_c^N}{r_c^{\bar{N}}} \propto \frac{\sigma^{\bar{N}}}{\sigma^N} = \frac{\frac{(m_A(r_c^{\bar{N}}) + m_B + m_C + m_D)g}{r_c^{\bar{N}} b}}{\frac{(m_A(r_c^N) + m_B + m_C)g}{r_c^N b}} = \frac{r_c^N}{r_c^{\bar{N}}} \frac{m_A(r_c^{\bar{N}}) + m_B + m_C + m_D}{m_A(r_c^N) + m_B + m_C}$$

331

332

$$\Rightarrow 1 = \frac{m_A(r_c^{\bar{N}}) + m_B + m_C + m_D}{m_A(r_c^N) + m_B + m_C}$$

333

$$\Rightarrow m_A(r_c^N) = m_A(r_c^{\bar{N}}) + m_D \quad (\text{B2})$$

334

By inserting the formulations for m_A (equation A1), the formula to correct an imprecisely cut N-PST is derived as:

$$335 \quad r_c^N = \frac{r_c^{\bar{N}} b \sum_{i=1}^N h_i \rho_i + b \tan(\beta) \sum_{i=1}^N \frac{h_i^2 \rho_i}{2} + (z_N - z_i) h_i \rho_i}{b \sum_{i=1}^N h_i \rho_i}$$
$$336 \quad = r_c^{\bar{N}} + \frac{\tan(\beta) \sum_{i=1}^N \frac{h_i^2 \rho_i}{2} + (z_N - z_i) h_i \rho_i}{\sum_{i=1}^N h_i \rho_i} \quad (\text{B3})$$

337



338 **Appendix C:**

339 **Table C1: Results of 27 pairs of PSTs, critical cut lengths r_c^V and r_c^N indicate whether PST beam ends were cut vertical or slope**
 340 **normal. Slab thickness H^N was measured in slope normal direction. Slope angle is provided in degrees. For further snowpack**
 341 **data we refer to the Appendix D.**

PST- pairs	Location Date	Critical cut length r_c^V (cm)	Critical cut length r_c^N (cm)	Slab thickness H^N (cm)	Slope angle (°)
1	Davos 1.12.21	55 (±2)	43 (±2)	62 (±2)	25 (±2)
2	Davos 1.12.21	49 (±2)	36 (±2)	62 (±2)	25 (±2)
3	Davos 1.12.21	47 (±2)	41 (±2)	62 (±2)	25 (±2)
4	Davos 1.12.21	51 (±2)	37 (±2)	62 (±2)	25 (±2)
5	Davos 1.12.21	56 (±2)	46 (±2)	62 (±2)	25 (±2)
6	Davos 1.12.21	61 (±2)	45 (±2)	58 (±2)	25 (±2)
7	Davos 1.12.21	59 (±2)	41 (±2)	58 (±2)	25 (±2)
8	Davos 1.12.21	65 (±2)	47 (±2)	60 (±2)	25 (±2)
9	Davos 1.12.21	66 (±2)	49 (±2)	63 (±2)	25 (±2)
10	Davos 1.12.21	70 (±2)	49 (±2)	63 (±2)	25 (±2)
11	Davos 1.12.21	61 (±2)	42 (±2)	63 (±2)	25 (±2)
12	Davos 1.12.21	63 (±2)	52 (±2)	64 (±2)	25 (±2)
13	Davos 1.12.21	62 (±2)	42 (±2)	64 (±2)	25 (±2)
14	Davos 1.12.21	62 (±2)	49 (±2)	64 (±2)	25 (±2)
15	Davos 1.12.21	67 (±2)	45 (±2)	64 (±2)	25 (±2)
16	Davos 1.12.21	67 (±2)	51 (±2)	67 (±2)	25 (±2)
17	Davos 1.12.21	60 (±2)	45 (±2)	67 (±2)	25 (±2)
18	Bacon Rind 1.20.21	31 (±2)	25 (±2)	57 (±2)	29 (±2)
19	Bacon Rind 1.20.21	33 (±2)	21 (±2)	56 (±2)	30 (±2)
20	Bacon Rind 1.20.21	29 (±2)	16 (±2)	55 (±2)	30 (±2)
21	Bacon Rind 1.20.21	29 (±2)	18 (±2)	55 (±2)	29 (±2)
22	Bacon Rind 1.20.21	23 (±2)	17 (±2)	54 (±2)	29 (±2)
23	Bacon Rind 1.25.21	29 (±2)	15 (±2)	52 (±2)	30 (±2)
24	Bacon Rind 1.25.21	33 (±2)	15 (±2)	53 (±2)	30 (±2)
25	Bacon Rind 1.25.21	30 (±2)	14 (±2)	54 (±2)	30 (±2)
26	Mount Ellis 3.1.21	59 (±2)	38 (±2)	93 (±2)	25 (±2)
27	Mount Ellis 3.1.21	50 (±2)	29 (±2)	95 (±2)	25 (±2)

342

343



344 **Table C2: Critical cut lengths measured at Mount Ellis, Critical cut lengths r_c^{DOWN} and r_c^{UP} indicate if the weak layer was cut**
 345 **downslope or upslope, respectively. Slab thickness H^N was measured in slope normal direction. Slope angle is provided in de-**
 346 **grees. For further snowpack data we refer to the Appendix D.**

347

PST-pairs	Location Date	PST Geometry	Critical cut length r_c^{DOWN} (cm)	Critical cut length r_c^{UP} (cm)	Slab thickness H^N (cm)	Slope angle ($^\circ$)
1	Bacon Rind 1.25.21	Slope normal	49 (± 2)	15 (± 2)	50 (± 2)	30 (± 2)
2	Bacon Rind 1.25.21	Vertical	24 (± 2)	29 (± 2)	52 (± 2)	30 (± 2)
3	Bacon Rind 1.25.21	Slope normal	29 (± 2)	33 (± 2)	54 (± 2)	30 (± 2)
4	Bacon Rind 1.25.21	Vertical	50 (± 2)	50 (± 2)	53 (± 2)	30 (± 2)
5	Bacon Rind 1.25.21	Slope normal	33 (± 2)	14 (± 2)	53 (± 2)	30 (± 2)
6	Bacon Rind 1.25.21	Vertical	24 (± 2)	30 (± 2)	53 (± 2)	31 (± 2)

348

349

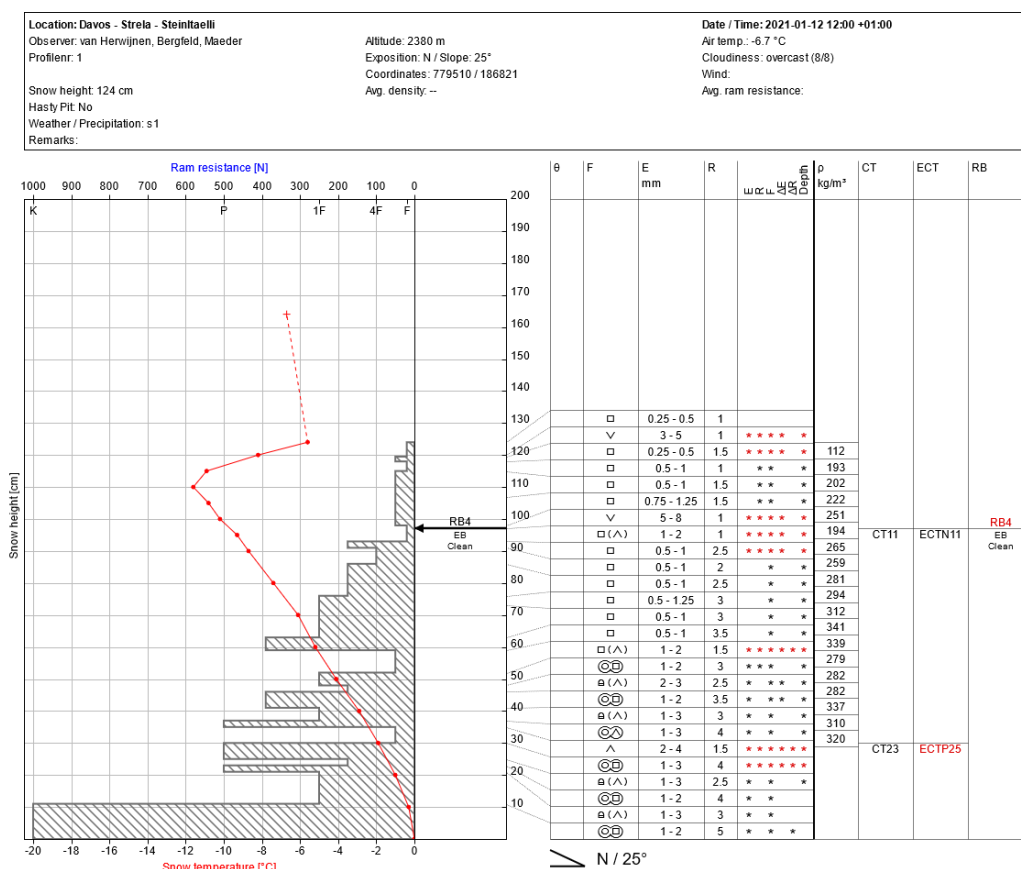


350 **Appendix D:**

351 At each of our four field sites we took a manual profile including density measures. The following four figures are excerpts

352 from the corresponding snow profile databanks.

353



354

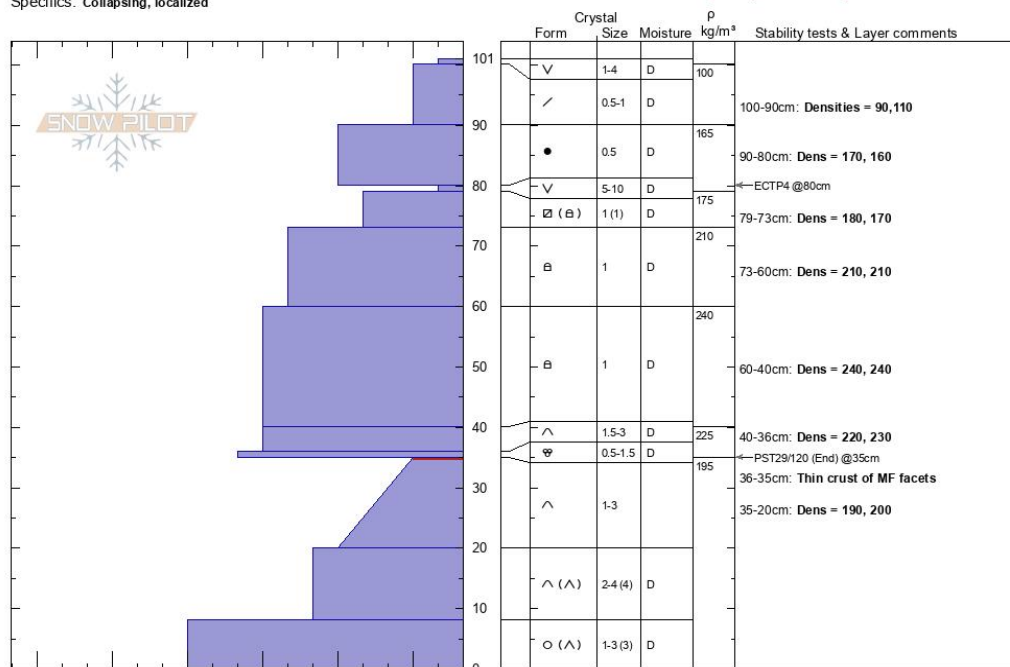
355 **Figure D1:** Manual profile taken at the Davos field site. The hashed area at the left site represents the hand hardness with snow
 356 height, the red line snow temperature with snow height. On the right side, grain type, grain size, hand harness, lemons and
 357 snow density are given. On the very right, stability test results are written at the height, of the tested weak layer.



Bacon Rind Sm Meadow Karl Birkeland
Bridger Range 01/20/2021 - 12:00pm
MT Co-ord: 44.88192N, -111.07457W
 Elevation: 2315 m Slope Angle: 30°
 Aspect: 90° Wind Loading: no
 Specifics: Collapsing, localized

Stability: HS: 101
 Air Temperature: PF: 90
 Sky Cover: CLR
 Precipitation: NO
 Wind: Calm

Layer Notes:
 100-90cm: Densities = 90,110
 90-80cm: Dens = 170, 160
 79-73cm: Dens = 180, 170
 73-60cm: Dens = 210, 210
 60-40cm: Dens = 240, 240
 [More Layer Comments below]



Notes: Pit dug to document snow conditions for research on PST geometry.. Additional Layer Comments: 36-40cm: Dens = 220, 230; 35-36cm: Thin crust of MF facets; 20-35cm: Dens = 190, 200; 20-35cm: Problematic layer;

358

359

360

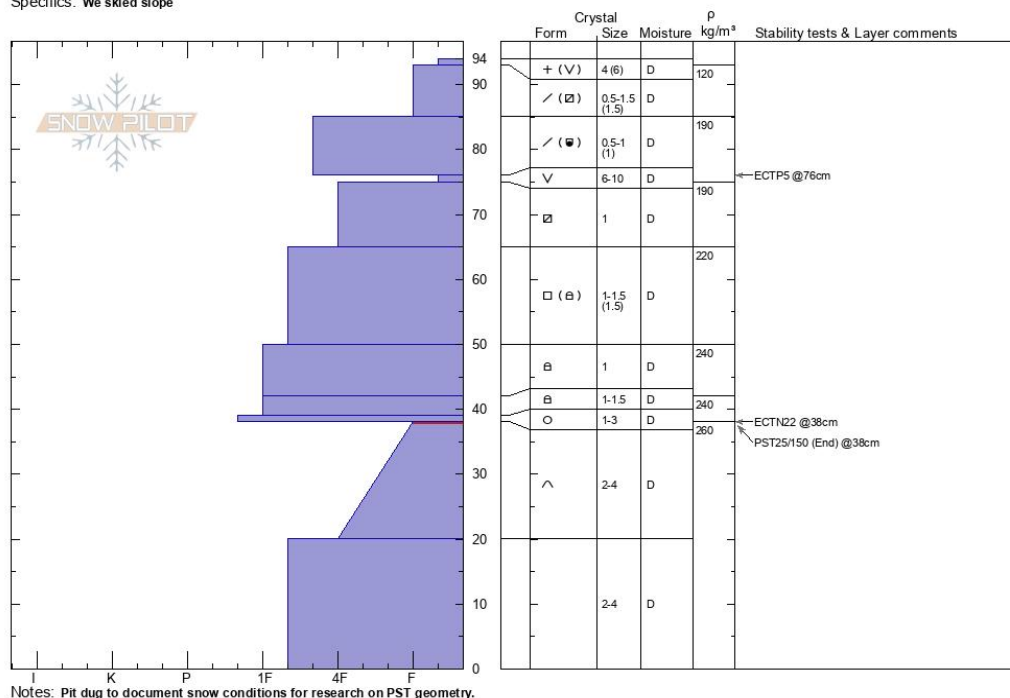
361

Figure D2: Manual profile taken at the Bacon Rind field site on January 20th 2021. The blue area at the left site represents the hand hardness with snow height, On the right side, grain type, grain size, moisture and snow density are given. On the very right, stability test results are written at the height, of the tested weak layer.



Bacon Rind Sm Meadow Karl Birkeland
Madison Range-S 01/25/2021 - 12:00pm
MT Co-ord: 44.84934N, -111.07942W
 Elevation: 2321 m Slope Angle: 30°
 Aspect: 80° Wind Loading:
 Specifics: We skied slope

Stability: HS: 94 Layer Notes: 38-20cm: Problematic layer
 Air Temperature:
 Sky Cover: CLR
 Precipitation: NO
 Wind: Calm



362

363 **Figure D3: Manual profile taken at the Bacon Rind field site on January 25th. The blue area at the left site represents the hand**
 364 **hardness with snow height, On the right side, grain type, grain size, moisture and snow density are given. On the very right,**
 365 **stability test results are written at the height, of the tested weak layer.**

366

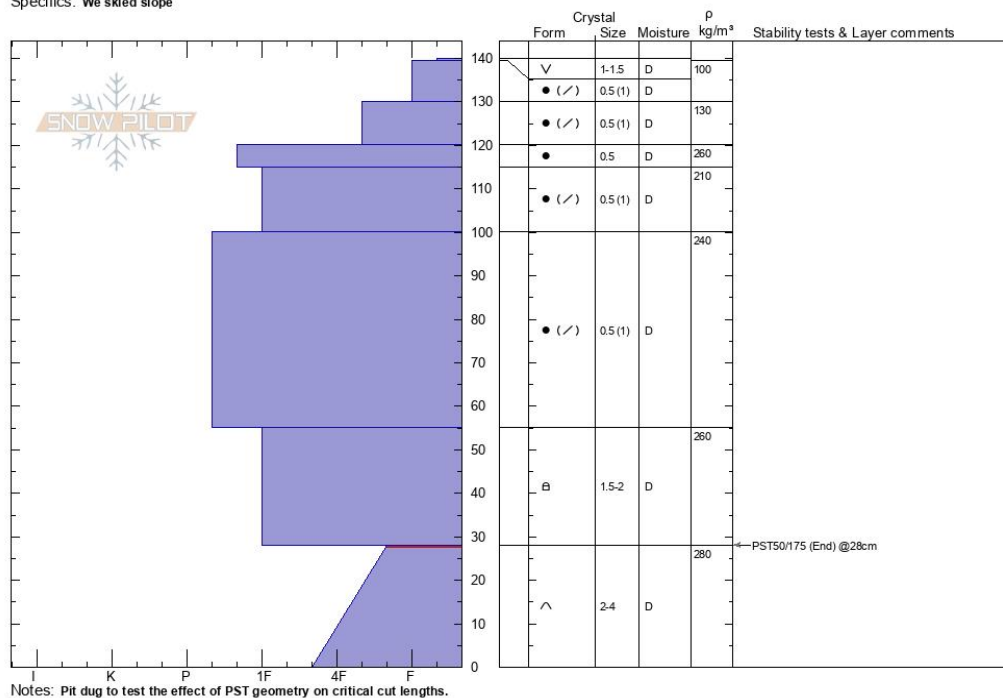


Mt Ellis
Gallatin Range-N
MT
 Elevation: **2439 m**
 Aspect: **25°**
 Specifics: **We skied slope**

Karl Birkeland
03/01/2021 - 12:00pm
 Co-ord: **45.58173N, -110.95616W**
 Slope Angle: **27°**
 Wind Loading:

Stability: **HS: 140**
 Air Temperature:
 Sky Cover: **CLR**
 Precipitation: **NO**
 Wind: **Calm**

Layer Notes:
 28-0cm: **Problematic layer**



367

368 **Figure D4: Manual profile taken at the Mount Ellis field site on January 25th. The blue area at the left site represents the hand**
 369 **hardness with snow height, On the right side, grain type, grain size, moisture and snow density are given. On the very right,**
 370 **stability test results are written at the height, of the tested weak layer.**

371

372 **Competing interests**

373 The contact author has declared that none of the authors has any competing interests

374 **Acknowledgement**

375 We would like to thank Flavia Maeder, Erika Birkeland, and Alex Marienthal for assisting in the field. This research was
 376 partly supported by the Swiss National Science Foundation (grant no. 200021_169424) and funded by the Deutsche For-
 377 schungsgemeinschaft (DFG, German Research Foundation) under grant no. 460195514.



378 **REFERENCES**

- 379 Bair, E.H., Simenhois, R., van Herwijnen, A. and Birkeland, K., 2014. The influence of edge effects on crack propagation in snow stability
380 tests. *The Cryosphere*, 8(4): 1407-1418.
- 381 Bair, E.H., Simenhois, R., van Herwijnen, A. and Birkeland, K.W., 2013. Edge effects in propagation tests. In: F. Naaim-Bouvet, Y. Durand
382 and R. Lambert (Editors), *Proceedings ISSW 2013. International Snow Science Workshop*, Grenoble, France, 7-11 October
383 2013. ANENA, IRSTEA, Météo-France, Grenoble, France, pp. 335-356.
- 384 Bergfeld, B., van Herwijnen, A., Bobillier, G., Larose, E., Moreau, L., Trotter, B., Gaume, J., Cathomen, J., Dual, J. and Schweizer, J.,
385 2022. Crack propagation speeds in weak snowpack layers. *Journal of Glaciology*, 68(269): 557-570.
- 386 Bergfeld, B., van Herwijnen, A., Bobillier, G., Rosendahl, P.L., Weißgraeber, P., Adam, V., Dual, J. and Schweizer, J., 2023. Temporal
387 evolution of crack propagation characteristics in a weak snowpack layer: conditions of crack arrest and sustained propagation.
388 *Natural Hazards and Earth System Sciences*, 23(1): 293-315.
- 389 Bergfeld, B., van Herwijnen, A., Reuter, B., Bobillier, G., Dual, J. and Schweizer, J., 2021. Dynamic crack propagation in weak snowpack
390 layers: insights from high-resolution, high-speed photography. *The Cryosphere*, 15(7): 3539-3553.
- 391 Birkeland, K.W., van Herwijnen, A., Reuter, B. and Bergfeld, B., 2019. Temporal changes in the mechanical properties of snow related to
392 crack propagation after loading. *Cold Regions Science and Technology*, 159: 142-152.
- 393 CAA, 2016. *Technical Aspects of Snow Avalanche Risk Management—Resources and Guidelines for Avalanche Practitioners in Canada*,
394 Canadian Avalanche Association, Revelstoke, BC, Canada.
- 395 Fierz, C., Armstrong, R.L., Durand, Y., Etchevers, P., Greene, E., McClung, D., Nishimura, K., Satyawali, P.K. and Sokratov, S., 2008.
396 The 2008 international classification of seasonal snow on the ground. In: C. Campbell, S. Conger and P. Haegeli (Editors),
397 *Proceedings ISSW 2008. International Snow Science Workshop*, Whistler, Canada, 21-27 September 2008, pp. 579-580.
- 398 Gaume, J., van Herwijnen, A., Chambon, G., Wever, N. and Schweizer, J., 2017. Snow fracture in relation to slab avalanche release:
399 critical state for the onset of crack propagation. *The Cryosphere*, 11(1): 217-228.
- 400 Gauthier, D. and Jamieson, B., 2008a. Evaluation of a prototype field test for fracture and failure propagation propensity in weak snowpack
401 layers. *Cold Regions Science and Technology*, 51(2-3): 87-97.
- 402 Gauthier, D. and Jamieson, B., 2008b. Fracture propagation propensity in relation to snow slab avalanche release: Validating the
403 Propagation Saw Test. *Geophysical Research Letters*, 35(13): L13501.
- 404 Gauthier, D. and Jamieson, J.B., 2006a. Evaluating a prototype field test for weak layer fracture and failure propagation. In: J.A. Gleason
405 (Editor), *Proceedings ISSW 2006. International Snow Science Workshop*, Telluride CO, U.S.A., 1-6 October 2006, pp. 107-116.
- 406 Gauthier, D. and Jamieson, J.B., 2006b. Towards a field test for fracture propagation propensity in weak snowpack layers. *Journal of*
407 *Glaciology*, 52(176): 164-168.
- 408 Greene, E., Birkeland, K.W., Elder, K., McCammon, I., Staples, M., Sharaf, D., Trautman, S. and Wagner, W., 2022. *Snow, Weather, and*
409 *Avalanches: Observation Guidelines for Avalanche Programs in the United States*. American Avalanche Association, Denver
410 CO, U.S.A., 110 pp.
- 411 Heierli, J., Gumbsch, P. and Zaiser, M., 2008. Anticrack nucleation as triggering mechanism for snow slab avalanches. *Science*,
412 321(5886): 240-243.
- 413 Jamieson, J.B. and Johnston, C.D., 1998. Refinements to the stability index for skier-triggered dry slab avalanches. *Annals of Glaciology*,
414 26: 296-302.
- 415 McClung, D.M., 2009. Dry snow slab quasi-brittle fracture initiation and verification from field tests. *Journal of Geophysical Research-*
416 *Earth Surface*, 114: F01022.
- 417 Morin, S., Horton, S., Techel, F., Bavay, M., Coléou, C., Fierz, C., Gobiet, A., Hagenmuller, P., Lafaysse, M., Ližar, M., Mitterer, C., Monti,
418 F., Müller, K., Oiefs, M., Snook, J.S., van Herwijnen, A. and Vionnet, V., 2020. Application of physical snowpack models in
419 support of operational avalanche hazard forecasting: A status report on current implementations and prospects for the future.
420 *Cold Regions Science and Technology*, 170: 102910.
- 421 Richter, B., Schweizer, J., Rotach, M.W. and van Herwijnen, A., 2019. Validating modeled critical crack length for crack propagation in
422 the snow cover model SNOWPACK. *The Cryosphere*, 13(12): 3353-3366.
- 423 Rosendahl, P.L. and Weissgraeber, P., 2020. Modeling snow slab avalanches caused by weak-layer failure - Part 1: Slabs on compliant
424 and collapsible weak layers. *The Cryosphere*, 14(1): 115-130.
- 425 Schweizer, J., Reuter, B., van Herwijnen, A. and Gaume, J., 2016. Avalanche release 101. In: E. Greene (Editor), *Proceedings ISSW*
426 *2016. International Snow Science Workshop*, Breckenridge CO, U.S.A., 3-7 October 2016, pp. 1-11.
- 427 Sigrist, C. and Schweizer, J., 2007. Critical energy release rates of weak snowpack layers determined in field experiments. *Geophysical*
428 *Research Letters*, 34(3): L03502.
- 429 Simenhois, R. and Birkeland, K.W., 2008. The effect of changing slab thickness on fracture propagation. In: C. Campbell, S. Conger and
430 P. Haegeli (Editors), *Proceedings ISSW 2008. International Snow Science Workshop*, Whistler, Canada, 21-27 September
431 2008, pp. 755-760.
- 432 van Herwijnen, A., Gaume, J., Bair, E.H., Reuter, B., Birkeland, K.W. and Schweizer, J., 2016. Estimating the effective elastic modulus
433 and specific fracture energy of snowpack layers from field experiments. *Journal of Glaciology*, 62(236): 997-1007.
- 434 Weißgraeber, P. and Rosendahl, P.L., 2023. A closed-form model for layered snow slabs. *The Cryosphere*, 17(4): 1475-1496.
- 435